2.HIGH-STRENGTH FLEXURAL REINFORCEMENT IN REINFORCED CONCRETE FLEXURAL MEMBERS UNDER MONOTONIC LOADING

by Leonardus Setia Budi Wibowo

Submission date: 08-Mar-2019 03:46AM (UTC-0500)
Submission ID: 1089884970
File name: REINFORCED_CONCRETE_FLEXURAL_MEMBERS_UNDER_MONOTONIC_LOADING.pdf (3.42M)
Word count: 6708
Character count: 34563

ACI STRUCTURAL JOURNAL TECHNICAL PAPER

Title No. 112-S65

High-Strength Flexural Reinforcement in Reinforced Concrete Flexural Members under Monotonic Loading

by Marnie B. Giduquio, Min-Yuan Cheng, and Leonardus S. B. Wibowo

This paper evaluates the performance of reinforced concrete (RC) flexural members reinforced with two different types of high-strength steels—Grade 100 A1035 and SD685—under monotonic loading. Test results indicate that design concepts of the current ACI Building Code can be used to evaluate the strength of specimens reinforced with either type of high-strength flexural reinforcement. With similar design parameters, specimens reinforced with high-strength flexural reinforcement exhibit equivalent ultimate displacement to those with conventional Grade 60 steel. Specimen behavior is greatly influenced by the buckling of compression reinforcement after spalling of cover concrete in the compression zone. The maximum spacing of transverse reinforcement (Grade 60) not exceeding $8d_b$ is suggested to restrain either SD685 or A1035 high-strength longitudinal reinforcement against premature buckling in flexural members primarily subjected to gravity-type loading, where d_b is the diameter of smallest compression reinforcement.

Keywords: deformation capacity; flexural strength; high-strength steel.

INTRODUCTION

The demand of high-rise buildings in several urban areas has increased dramatically in recent years. Driven by economic advantages and improvement in seismic performance (Liel et al. 2011), reinforced concrete (RC) has become the favored construction material for high-rise buildings. The effort to maintain reasonable member sizes often results to heavy reinforcing bar congestion, which is always significantly challenging to handle during construction, adversely affecting construction speed and quality. The use of high-strength steels has the potential to mitigate this issue (Aoyama 2001; Mast et al. 2008; Sumpter et al. 2009; Shahrooz et al. 2011, 2014; Harries et al. 2012). Different high-strength steels have been developed with distinct stress-strain characteristics.

Despite the encouraging results concerning the use of high-strength steel, most of the existing research studies focus only on one type of steel at a time. Test results comparing behavior of RC members reinforced with different types of high-strength steels are relatively limited. This study aims to fill the gap. Two types of high-strength steels are evaluated, namely, Grade 100 A1035 (ASTM A1035/A1035M 2011). Both steels have specified yield strengths of 100 ksi (690 MPa).

The relevant research and design guidelines for using A1035 steel are well-documented by ACI Innovation Task Group 6 (2010). In addition to its higher strength properties, A1035 steel features better corrosion resistance due to its low carbon and high chromium composition. The stress-strain relationship for A1035 steel proposed by ACI Innovation Task Group 6 (2010) is presented in Eq. (1). Relevant research for using SD685 can be found elsewhere (Aoyama 2001). The typical stress-strain relationship of SD685 steel is presented in Eq. (2) (Wang et al. 2009). The required material properties for A1035 and SD685 high-strength steels are summarized in Table 1 along with the conventional Grade 60 steel conforming to ASTM A706/706M (2009). One of the remarkable differences between the two high-strength steels is that SD685 steel exhibits a distinct yield plateau with a minimum steel strain of 0.014 before the onset of strain hardening (Aoyama 2001), whereas A1035 steel does not display a well-defined yield plateau. For comparison and design purposes, the stress-strain model for Grade 60 steel (Priestley et al. 1996) is presented in Eq. (3). The theoretical stress-strain curves based on Eq. (1), (2), and (3) are illustrated in Fig. 1.

$$\begin{cases} f_s = 29{,}000\varepsilon_s \ \text{(ksi)} & \text{for } 0 \le \varepsilon_s \le 0.0024 \\ f_s = 170 - \dfrac{0.43}{\varepsilon_s + 0.0019} \ \text{(ksi)} & \text{for } 0.0024 \le \varepsilon_s \le 0.0200 \\ f = 150 \ \text{(ksi)} & \text{for } 0.02 \le \varepsilon_s \le 0.06 \end{cases} \quad (1)$$

$$\begin{cases} f_s = 29{,}000\varepsilon_s \ \text{(ksi)} & \text{for } 0 \le \varepsilon_s \le 0.00345 \\ f_s = 100 \ \text{(ksi)} & \text{for } 0.00345 \le \varepsilon_s \le 0.01 \\ f = 138 - 38\left(\dfrac{0.097 - \varepsilon_s}{0.087}\right)^2 \ \text{(ksi)} & \text{for } 0.01 \le \varepsilon_s \le 0.097 \end{cases} \quad (2)$$

$$\begin{cases} f_s = 29{,}000\varepsilon_s \ \text{(ksi)} & \text{for } 0 \le \varepsilon_s \le 0.00207 \\ f_s = 60 \ \text{(ksi)} & \text{for } 0.00207 \le \varepsilon_s \le 0.008 \\ f = 60\left[1.5 - 0.5\left(\dfrac{0.12 - \varepsilon_s}{0.112}\right)^2\right] \ \text{(ksi)} & \text{for } 0.008 \le \varepsilon_s \le 0.12 \end{cases} \quad (3)$$

Flexural responses of RC beam specimens using conventional Grade 60, SD685, and A1035 steels as flexural reinforcement were experimentally studied. Five pairs of RC beam specimens were tested under a monotonically increasing gravity-type loading. Test results of all specimens are collectively discussed.

ACI Structural Journal, V. 112, No. 6, November-December 2015.
MS No. S-2014-126.R5, doi: 10.14359/51688057, received March 4, 2015 and reviewed under Institute publication policies.

Table 1—Required material properties of reinforcement

Bar type	Bar size	Minimum ε_{sh}, %	Minimum ε_{su}, %	Minimum f_y, ksi (MPa)	Minimum f_u, ksi (MPa)
ASTM A706 (Grade 60)	No. 3 to No. 6	NA	14	60 (414)	80 (550)*
	No. 7 to No. 11		12		
	No. 14 and No. 18		10		
SD685	All sizes	1.4	10	100 (690)	>1.25f_y
A1035	No. 3 to No. 11	NA	7	100 (690)†	150 (1035)
	No. 14 and No. 18		6		

*The value of f_u shall not be less than 1.25f_y.

†Determined using 0.2% offset method.

Table 2—Specimen design parameters

Specimen		Specified material properties				Using bilinear stress-strain and equivalent concrete stress block		Using Eq. (1) to (4)	
Group	Label	f_c', ksi (MPa)	Bar type	f_y, ksi (MPa)	Top/bottom bars	$\varepsilon_{t,b1}$, %	$M_{n,b1}$, kip-ft (kN-m)	$\varepsilon_{t,a1}$, %	$M_{n,a1}$, kip-ft (kN-m)
Control	C1 and C2	4 (28)	Grade 60	60 (414)	Two No. 5 Four No. 9	0.48	262.6 (356.1)	0.51	262.7 (356.2)
I-Group	I-S1 and I-S2	4 (28)	SD685	100 (690)	Two No. 4 Three No. 8	0.45	257.4 (348.9)	0.48	257.5 (349.1)
	I-A1 and I-A2	4 (28)	A1035	100 (690)	Two No. 4 Three No. 8	0.45	257.4 (348.9)	0.46	264.5 (358.6)
II-Group	II-S1 and II-S2	5 (35)	SD685	100 (690)	Two No. 5 Three No. 8	0.70	271.0 (367.5)	0.79	270.9 (367.3)
	II-A1 and II-A2	6 (42)	A1035	100 (690)	Two No. 8 Three No. 8	0.97	277.7 (376.5)	0.84	347.9 (471.7)

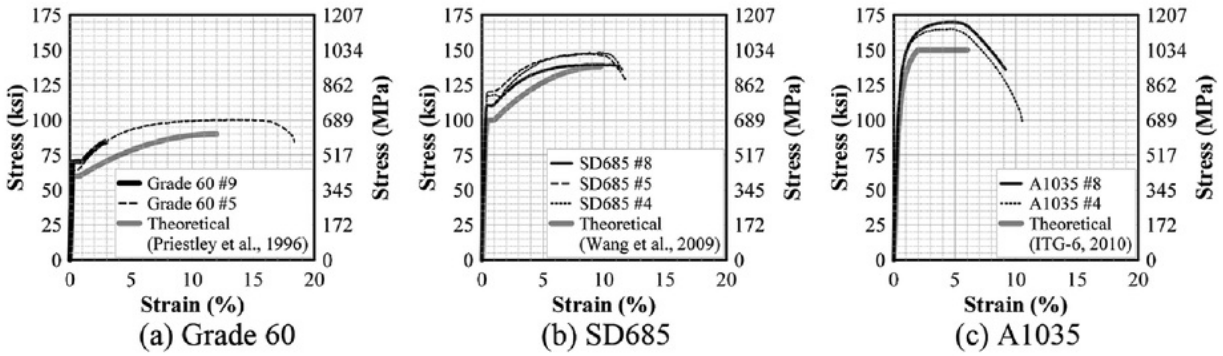

Fig. 1—Flexural reinforcement stress-strain relationship.

RESEARCH SIGNIFICANCE

Flexural behaviors of RC beam specimens reinforced with Grade 60, SD685, and Grade 100 A1035 steels were studied. The potential of using high-strength flexural reinforcement with different stress-strain characteristics in RC flexural members is evaluated. Test results will provide valuable information for the development of design recommendations of the future building codes.

TEST SPECIMENS

Five pairs of RC beam specimens were tested. Each pair of specimens was identically designed to verify the consistency of the test results. Specimens were designed using the steel stress-strain models from Eq. (1), (2), and (3), and the concrete stress-strain model from Eq. (4). Table 2 summarizes some important design parameters of each pair of test specimens. Design parameters using equivalent stress block model for concrete and elastic-perfectly-plastic steel properties are also presented. Control specimens, C1 and C2, were designed to satisfy the minimum requirement for a tension-controlled section—that is, the outermost steel tensile strain is 0.005 as the extreme concrete compressive strain reaches 0.003 per ACI 318-14. The cross-sectional dimensions of the control specimens were 11.8 in. (300 mm) wide and 18.1 in. (460 mm) deep. With concrete a compressive strength of 4 ksi (28 MPa), two No. 5 compression reinforcement and four No. 9 tension reinforcement were provided.

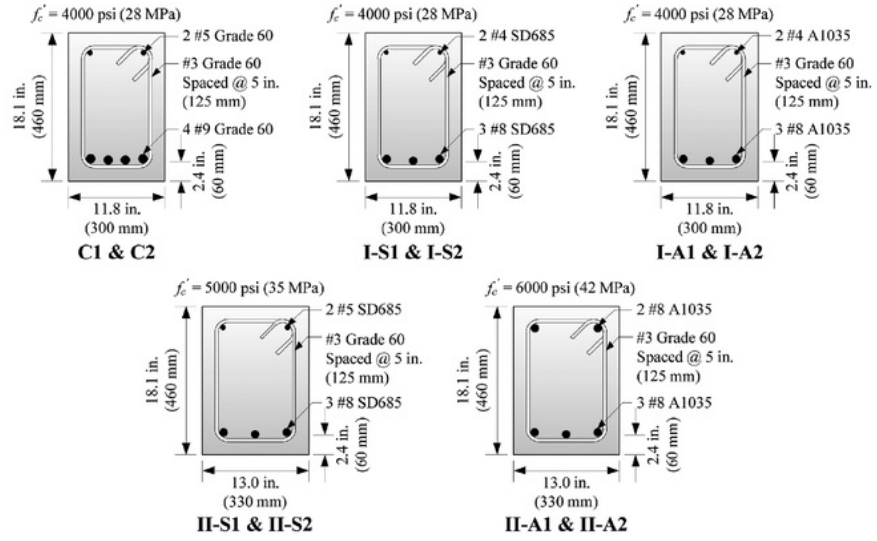

(a) Specimen Cross-Section

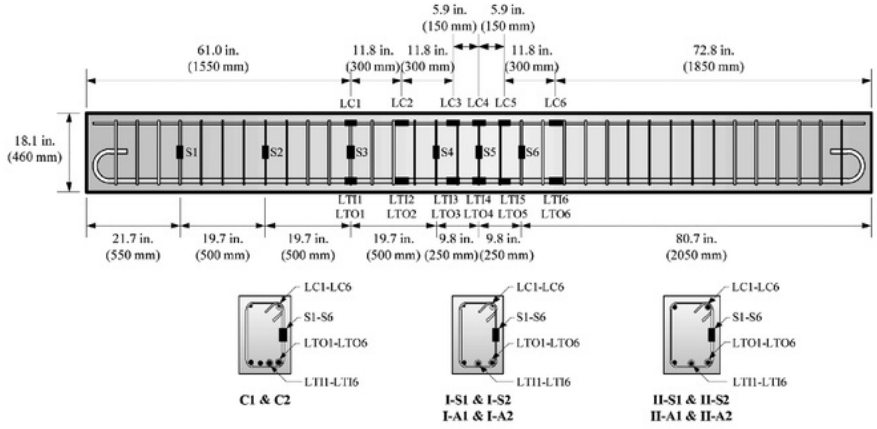

(b) Strain Gauge Detail

Fig. 2—Reinforcement layout and strain gauge detail.

$$\begin{cases} f_c = f_c' \left[2\left(\frac{\varepsilon_c}{0.002}\right) - \left(\frac{\varepsilon_c}{0.002}\right)^2 \right] & \text{for } 0 \le \varepsilon_s \le 0.002 \\ f = f_c' \left[1 - 150(\varepsilon_c - 0.002)\right] & \text{for } 0.002 \le \varepsilon_s \le 0.003 \end{cases} \quad (4)$$

Using equivalent force relationship $(A_s f_y)_{60\ ksi} = (A_s f_y)_{100\ ksi}$, the I-Group specimens were reinforced with two No. 4 compression reinforcement and three No. 8 tension reinforcement. It should be noted that the designed reinforcing bar tensile strain associated with the nominal flexural strength in the I-Group specimens was roughly the same as the control specimens. Test specimens in the II-Group were designed for a reinforcing bar tensile strain of 0.008 at nominal—a tension-controlled limit suggested by Shahrooz et al. (2011) for A1035 steel. The specimen widths were modified to 13.0 in. (330 mm) and the specified concrete strengths of specimen pairs II-S1/S2 and II-A1/A2 were adjusted to 5 and 6 ksi (35 and 42 MPa), respectively. As can be seen in Table 2, reinforcing bar tensile strain at nominal is sensitive to the selected material models, especially for speciment pair II-A1/A2.

Shear reinforcement, using No. 3 Grade 60 steel, was provided with 5 in. (125 mm) spacing to ensure flexure-governed behavior for all test specimens. The spacing of transverse reinforcement s was equivalent to $7.8d_b$ in specimen pairs C1/C2 and II-S1/S2, $9.6d_b$ in specimen pairs I-S1/S2 and I-A1/A2, and $5d_b$ in specimen pair II-A1/A2, wherein d_b is the diameter of smallest compression reinforcement. Reinforcement layouts for all test specimens are presented in Fig. 2.

EXPERIMENTAL SETUP AND TEST PROCEDURE

All specimens were tested under a four-point loading experimental setup, as shown in Fig. 3. The span length L between simple supports was 157.5 in. (4000 mm). The two concentrated loads, 31.5 in. (800 mm) apart, were applied symmetrically from the midspan. This test setup provided a

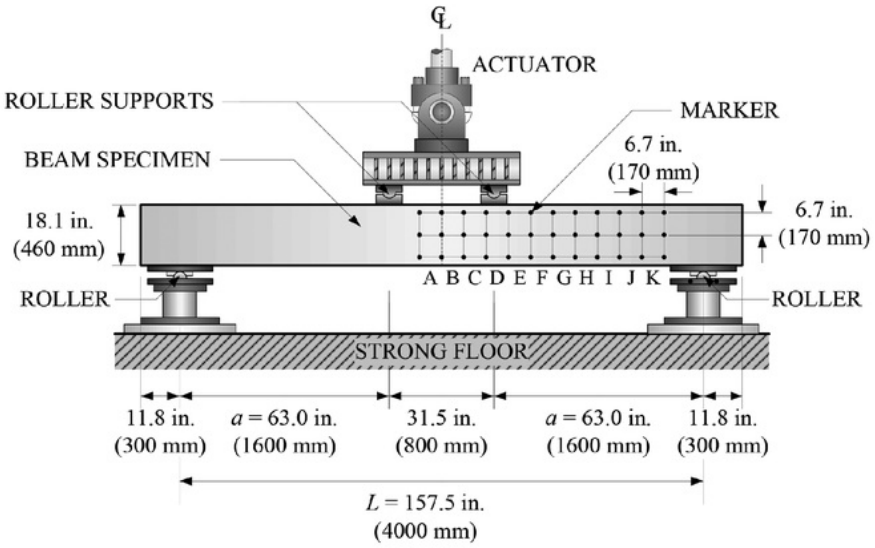

Fig. 3—Experimental setup.

Table 3—Summary of concrete cylinder strengths

Group	Control		I-Group				II-Group			
Specimen	C1	C2	I-S1	I-S2	I-A1	I-A2	II-S1	II-S2	II-A1	II-A2
f_c', ksi (MPa)	4773 (32.9)	4814 (33.2)	4762 (32.8)	4963 (34.2)	4686 (32.3)	4996 (34.4)	5589 (38.5)	5668 (39.1)	6441 (44.4)	6501 (44.8)

shear span to effective depth ratio (a/d) of approximately 4.0 for all test specimens.

The load was applied monotonically through a 220 kip (100 tonf) actuator at a constant rate of 0.004 in./s (0.1 mm/s). The crack widths of each specimen were measured at every 0.16 in. (4 mm) displacement increment. The displacement used in this paper corresponds to the displacement at the loading points, which is equivalent to the actuator's vertical displacement. Test was terminated when the load dropped by more than 20% from the peak. For each pair of specimens, the development of concrete strength was carefully monitored using a number of 4 x 8 in. (100 x 200 mm) concrete cylinders to assure the desired concrete strength on the testing date.

INSTRUMENTATION

A total of 24 strain gauges were attached to the surface of the reinforcing steel to measure steel strain at designated locations. The strain gauge layout is presented in Fig. 2(b). External deformation of each specimen was monitored using an optical tracking system with a specified resolution of 4×10^{-4} in. (0.01 mm). A total of 38 markers were used for each specimen: 36 are attached to the specimen in a 6.7 in. (170 mm) regular grid pattern while the remaining two were placed at the support to monitor support movement during the test. The relative marker positions are depicted in Fig. 3.

TEST RESULTS

Materials

Specimens with similar specified concrete strengths were cast together with the same concrete mixture. For all concrete mixtures, the maximum aggregate size was kept to 3/4 in. (19 mm). Concrete strengths presented in Table 3 were determined using the average strength of six 4 x 8 in. (100 x 200 mm) cylinder samples that were tested on the same day with the beam specimen. Mechanical properties of the flexural reinforcement were determined by direct tensile test. The representative stress-strain relationships of coupon samples are shown in Fig. 1. A summary of flexural reinforcement properties is provided in Table 4. Reinforcing bar fracture strain is defined at a point on the stress-strain curve corresponding to a 10% drop from peak stress (ASTM A370 2012).

Response of test specimens

All specimens failed in flexure based on the observed failure mechanism. The control specimens, I-Group specimens and specimen pair II-S1/S2 failed due to the combination of buckling of compression reinforcement and concrete crushing in the compression zone within the constant-moment span, as shown in Fig. 4. Due to severe buckling, one of the compression reinforcement of II-S2 fractured at the kink. It is also evident in Fig. 4 that buckling of compression reinforcement in the control specimens, I-Group specimens and specimen pair II-S1/S2 were all observed in between the two adjacent transverse reinforcement. Specimen pair II-A1/A2 failed due to fracture of tension reinforcement. Buckling of compression reinforcement was not observed in specimen pair II-A1/A2.

The load-displacement responses of all test specimens are presented in Fig. 5. Typically, each response curve consists of five key points and can be illustrated by the idealized curve shown in Fig. 5(a). Point A represents the onset of yielding of the tension reinforcement. For specimens with flexural reinforcement having a distinct yield

Table 4—Summary of flexural reinforcement properties

Bar type	Bar size	Yield			Peak		Ultimate		
		f_y, ksi (MPa)	ε_y, %	ε_{sh}, %	f_u, ksi (MPa)	ε_u, %	f_{su}, ksi (MPa)	ε_{su}, %	f_u/f_y
Grade 60	No. 5	64.0 (441.5)	0.24	0.56	100.2 (690.7)	13.27	90.2 (621.9)	17.50	1.6
	No. 9	70.2 (484.1)	0.24	0.94	NA*	NA*	NA*	NA*	NA*
SD685	No. 4	117.1 (807.7)	0.38	1.65	148.3 (1022.5)	9.43	138.6 (955.6)	11.13	1.3
	No. 5	120.0 (827.7)	0..41	1.13	147.2 (1015.1)	8.45	132.5 (913.6)	11.26	1.2
	No. 8	110.0 (758.4)	0.38	0.84	139.6 (962.7)	9.80	138.2 (952.5)	11.37	1.3
A1035	No. 4	132.3 (912.4)	0.66†	NA†	165.8 (1143.1)	4.73	149.2 (1028.7)	7.52	1.3
	No. 8	134.1 (924.4)	0.67†	NA†	170.0 (1171.9)	4.80	153.0 (1054.9)	6.31	1.3

*No data available. Tensile test was terminated before reaching peak load due to instrument limitations.

†Determined using 0.2% offset method.

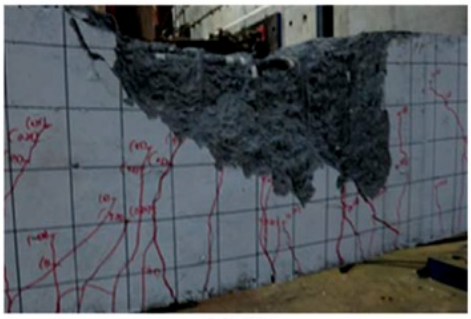

(a) C2

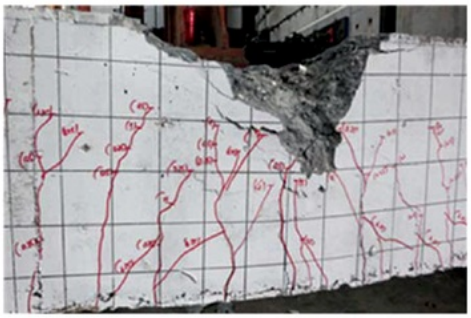

(b) I-S2

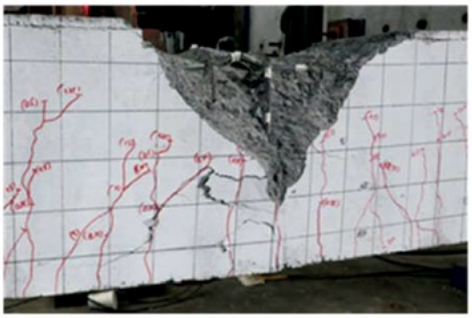

(c) I-A2

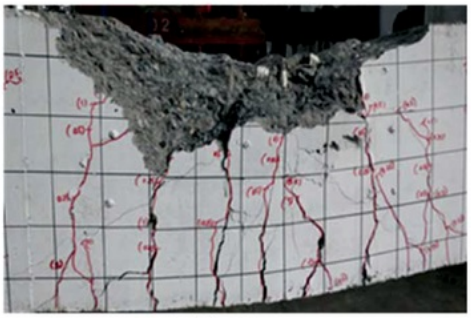

(d) II-S2

(e) II-A2

Fig. 4—Specimen state at end of test.

plateau, the load at Point A can be sustained up to Point B, which represents the first peak load prior to spalling of cover concrete in the compression zone. Immediately after Point B, the load suddenly drops to Point C. At this stage, compression reinforcement takes over a significant portion of the compression force and a stable segment is observed, wherein the load is roughly sustained up to Point D as the displacement increases. Some specimens may

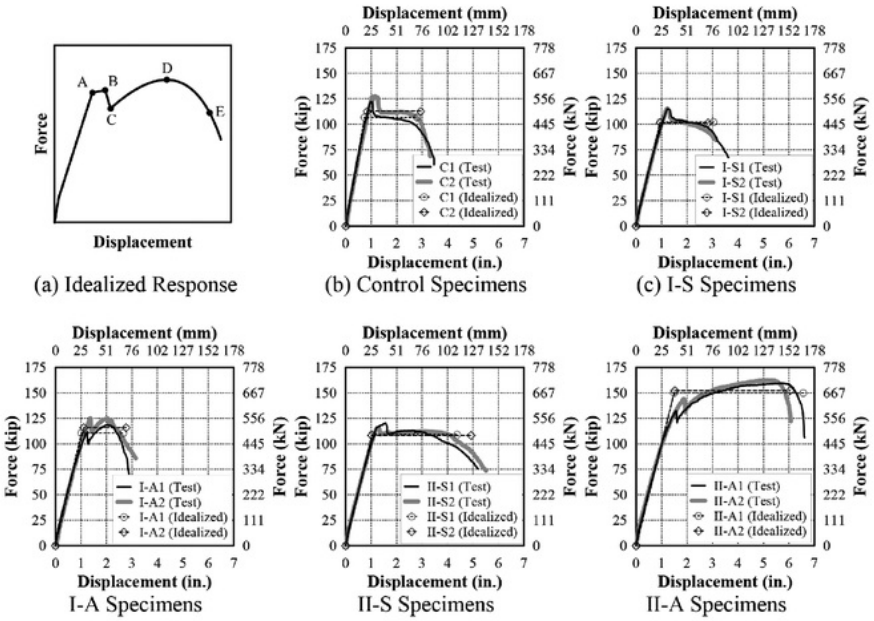

Fig. 5—Load-displacement response.

exhibit a gradual increase of load from Point C and reach the second peak at Point D, which is more pronounced for specimens reinforced with A1035. After Point D, the force starts to degrade and the specimen fails at Point E, which is referred to as the ultimate displacement point corresponding to a 20% load drop from the peak. Table 5 presents the numerical values of these key points along the load-displacement curve for each specimen. The theoretical nominal flexural strength $M_{n,b2}$ of each specimen, calculated using equivalent concrete stress block and bilinear steel stress-strain relationship using tested material properties, is also presented in Table 5.

Idealized bilinear responses

A bilinear force-displacement model is developed for each specimen to evaluate its flexural stiffness and displacement ductility. This idealized bilinear curve is developed as follows: The ultimate displacement Δ_E is defined at a point corresponding to 20% drop from the maximum force, and yield force P_y is determined by assuming an initial linear ascending portion intersecting the experimental load-displacement curve at 60% of P_y, providing equivalent areas below the idealized bilinear curve and the experimental load-displacement curve up to the ultimate displacement. The idealized bilinear response curve for each specimen is presented in Fig. 5. The numerical values of yield load, yield displacement, ultimate displacement and equivalent flexural rigidity ratio are summarized in Table 5. Equivalent flexural rigidity EI is determined based on elastic bending theory as $EI = P_y a^2(3L - 4a)/12\Delta_y$, where P_y is the idealized yield load, a is the shear span, L is the simple span, and Δ_y is the idealized yield displacement.

Flexural strength

Specimens in the I-Group exhibited roughly similar first peak loads with the control specimens. The average ratio between the experimental flexural strength M_B corresponding to the first peak load at Point B and theoretical nominal flexural strength of specimen pairs I-S1/S2 and I-A1/A2 are roughly unity. However, the load-displacement responses of specimen pair I-A1/A2 show notable post-yield stiffness after Point C. The second peak load of Specimen I-A1 is even greater than its first peak but not significant. For specimen pairs II-S1/S2 and II-A1/A2, the average ratio between the experimental flexural strength M_B and theoretical flexural strength is also approximately unity but the experimental flexural strengths M_D corresponding to the second peak loads of specimen pairs II-A1/A2 are approximately 15% higher than the corresponding theoretical values.

Test results suggest that flexural strengths of specimens using SD685 and A1035 high-strength longitudinal reinforcement may be adequately estimated using equivalent concrete stress block and elastic-perfectly-plastic steel properties per ACI 318-14, provided that steel yield stress is selected adequately. It should be noted that A1035 high-strength steel exhibits a tested-to-specified yield stress ratio greater than 1.3, which is considerably higher than the stress ratio of 1.1 observed in both Grade 60 and SD685 steels. The use of specified 100 ksi (690 MPa) yield strength for A1035 high-strength steel may underestimate flexural strength significantly.

Among all the test specimens, pairs I-A1/A2, II-S1/S2, and II-A1/A2 show hardening behavior after spalling of cover concrete—that is, $P_D \geq P_C$. It has been reported in previous research (Rashid and Mansur 2005; Lin and Lee 2001) that this hardening behavior is influenced by: 1) tension reinforcement ratio ρ; 2) compression-to-tension reinforcement ratio ρ'/ρ; 3) spacing of transverse reinforcement s; 4) concrete strength; and 5) beam cross section. Test results of specimen pairs I-S1/S2 and I-A1/A2 indicate that steel stress-strain characteristics are also crit-

Table 5—Summary of test results

Specimen	Group	Control		I-Group				II-Group			
	Mark	C1	C2	I-S1	I-S2	I-A1	I-A2	II-S1	II-S2	II-A1	II-A2
Point A	Δ_A, in. (mm)	0.98 (24.9)	1.04 (26.4)	1.23 (31.2)	1.22 (31.0)	NA	NA	1.21 (30.7)	1.22 (31.0)	NA	NA
	P_A, kip (kN)	122.2 (543.6)	127.2 (565.8)	114.8 (510.7)	115.3 (512.9)	NA	NA	115.7 (514.7)	115.4 (513.3)	NA	NA
Point B	Δ_B, in. (mm)	1.05 (26.7)	1.24 (31.5)	1.31 (33.3)	1.25 (31.8)	1.26 (32.0)	1.36 (34.5)	1.58 (40.1)	1.32 (33.5)	1.58 (40.1)	1.88 (47.8)
	P_B, kip (kN)	121.7 (541.3)	126.6 (563.1)	114.4 (508.9)	115.1 (512.0)	111.6 (496.4)	125.1 (556.5)	120.2 (534.7)	116.0 (516.0)	132.4 (588.9)	144.1 (641.0)
Point C	Δ_C, in. (mm)	1.15 (29.2)	1.41 (35.8)	1.49 (37.8)	1.44 (36.6)	1.29 (32.8)	1.40 (35.6)	1.65 (41.9)	1.37 (34.8)	1.61 (40.9)	1.93 (49.0)
	P_C, kip (kN)	108.1 (480.9)	110.9 (493.3)	105.7 (470.2)	103.4 (459.9)	99.7 (443.5)	111.6 (496.4)	110.1 (489.7)	109.2 (485.7)	120.8 (537.3)	130.8 (581.8)
Point D	Δ_D, in. (mm)	NA*	2.15 (54.6)	NA*	NA*	2.03 (51.6)	2.04 (51.8)	2.66 (67.6)	2.97 (75.4)	5.73 (145.5)	5.12 (130.0)
	P_D, kip (kN)	NA*	112.1 (498.6)	NA*	NA*	118.8 (528.4)	124.8 (555.1)	113.0 (502.6)	112.4 (500.0)	159.5 (709.5)	162.3 (721.9)
Point E	Δ_E, in. (mm)	2.79 (70.9)	2.94 (74.7)	3.04 (77.2)	2.83 (71.9)	2.66 (67.6)	2.77 (70.4)	4.38 (111.3)	4.92 (125.0)	6.56 (166.6)	6.04 (153.4)
	P_E, kip (kN)	97.8 (435.0)	102.8 (457.3)	91.8 (408.3)	92.2 (410.1)	95.0 (422.6)	100.1 (445.3)	96.2 (427.9)	92.8 (412.8)	127.6 (567.6)	129.9 (577.8)
Idealized yield point	Δ_y, in. (mm)	0.73 (18.5)	0.84 (21.3)	0.94 (23.9)	0.95 (24.1)	1.02 (25.9)	1.11 (28.2)	1.04 (26.4)	1.02 (25.9)	1.49 (37.8)	1.52 (38.6)
	P_y, kip (kN)	106.7 (474.6)	112.7 (501.3)	102.1 (454.2)	101.3 (450.6)	110.7 (492.4)	115.9 (515.5)	109.0 (484.9)	108.4 (482.2)	149.9 (666.8)	152.3 (677.5)
Test peak moment	M_{peak}, kip-ft (kN-m)	320.7 (434.8)	333.9 (452.7)	301.3 (408.5)	302.6 (410.3)	311.8 (422.7)	328.3 (445.1)	315.5 (427.8)	304.5 (412.8)	418.6 (567.5)	426.0 (577.6)
Nominal moment capacity	$M_{n,b2}$, kip-ft (kN-m)	307.2 (416.5)	307.6 (417.1)	286.6 (388.5)	288.5 (391.1)	302.8 (410.5)	312.9 (424.3)	298.5 (404.7)	299.0 (405.3)	365.3 (495.3)	365.6 (495.8)
Outermost tensile strain	$\varepsilon_{t,b2}$, %	0.45	0.45	0.47	0.49	0.41	0.42	0.67	0.68	0.69	0.69
Displacement ductility	Δ_E/Δ_y	3.82	3.50	3.23	2.98	2.61	2.50	4.21	4.82	4.40	3.97
Displacement deformability	Δ_E/Δ_{Ser}	5.64	5.60	5.05	4.45	4.07	4.07	6.64	7.58	8.01	7.38
Strength ratio	$M_B/M_{n,b2}$	1.04	1.08	1.05	1.05	0.97	1.05	1.06	1.02	0.95	1.03
	$M_D/M_{n,b2}$	NA*	0.96	NA*	NA*	1.03	1.05	0.99	0.99	1.15	1.17
Equivalent flexural rigidity ratio	EI/E_cI_g	0.46	0.42	0.34	0.33	0.35	0.32	0.28	0.28	0.25	0.25

*Specimen does not exhibit second peak load.

ical. It is believed that the absence of hardening behavior in certain specimens is primarily attributed to premature buckling of compression reinforcement.

Deformation

Specimen displacements are reported in Table 5. Displacement is contributed by both flexure and shear. Shear deformation of the second specimen of each specimen pair, obtained from measurements of optical markers from Columns E to K as depicted in Fig. 3, is presented in Fig. 6. It shows that 15 to 20% of the overall displacement at first peak load is developed by shear. Right after first peak load, percentage of shear deformation-to-overall deformation gradually drops. Specimen pairs I-A1/A1 and II-A1/A2, reinforced with A1035 steel, show a relatively higher shear displacement than the rest of the specimens.

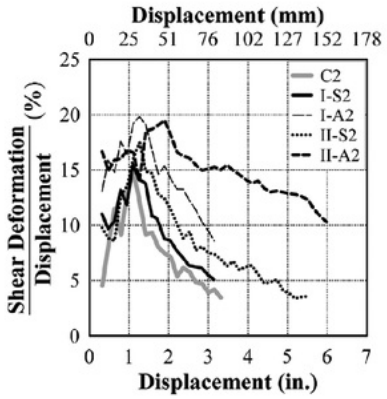

Fig. 6—Shear deformation contribution to overall displacement.

The control and I-Group specimens that have similar reinforcing bar tensile strain at nominal flexural strength ($\varepsilon_{t,b2} \approx 0.005$) but with transverse reinforcement at $7.8d_b$ and $9.6d_b$ spacing, respectively, exhibit comparable ultimate displacement Δ_E. The increased reinforcing bar tensile strain at nominal flexural strength to $\varepsilon_{t,b2} \approx 0.007$ and reduced spacing of transverse reinforcement substantially increase ultimate displacement of specimens in the II-Group.

Considering that most of the specimens failed due to buckling of compression reinforcement, it suggests that spacing of transverse reinforcement is a crucial factor that impacts specimen deformation capacity in addition to reinforcing bar tensile strain at nominal flexural strength. For flexural members not designed as part of the seismic-force-resisting system, ACI 318-14 requires spacing of Grade 60 transverse reinforcement not to exceed $16d_b$ to restrain longitudinal reinforcement against buckling, where d_b is the diameter of smallest compression reinforcement. However, buckling of compression reinforcement is still observed in the control specimens at early stage—that is, approximately concurrent with spalling of cover concrete. The $16d_b$ limit may need further review, especially when smaller-size compression reinforcement is used.

On the other hand, the I-Group specimens having transverse reinforcement at $9.6d_b$ spacing exhibited comparable ultimate displacement and identical failure mode as the control specimens. Reducing transverse reinforcement from $9.6d_b$ to $7.8d_b$ effectively inhibits premature buckling of SD685 high-strength steel in specimen pair II-S1/S2 after spalling of cover concrete. The A1035 high-strength steel is expected to have better buckling resistance due to its so-called "roundhouse" stress-strain characteristics. As a result, the maximum transverse reinforcement (Grade 60) spacing of $8d_b$ appears to be an adequate limit to restrain either SD685 or A1035 high-strength steel against premature buckling in flexural members primarily subjected to gravity-type loading. Only specimen pair II-A1/A2 failed without buckling of compression reinforcement throughout the test. Grade 60 transverse reinforcement at $5d_b$ spacing appears to be a conservative limit to prevent buckling of A1035 high-strength steel in flexural member subjected primarily to monotonic-type loading.

Based on experimental evidence outlined above, a flexural member using the studied high-strength longitudinal reinforcement is capable of achieving comparable ultimate displacement as the code-compliant flexural member under gravity-type loading, provided that flexural member using the studied high-strength reinforcement is designed to: 1) have similar reinforcing bar tensile strain at nominal flexural strength as the code-compliant flexural member; 2) have transverse reinforcement (Grade 60) spacing limited to 8 times the diameter of the minimum primary compression reinforcement; and 3) avoid shear-governed failure mode.

Deformation capacity of each specimen is further evaluated using two displacement indexes—namely, displacement ductility ratio Δ_E/Δ_y and displacement deformability ratio, Δ_E/Δ_{Ser}—where Δ_{Ser} is the specimen displacement under service load corresponding to $0.6M_{n,b2}$. Both ratios are also provided in Table 5. Previous research (Mast et al. 2008) indicates that deformability ratio may be a suitable indicator to measure deformation ability of specimen reinforced with high-strength longitudinal reinforcement. As presented in Table 5, both displacement ductility and deformability ratios of the I-Group specimens are smaller compared to those of the control specimens. The increase of $\varepsilon_{t,b2}$ to approximately 0.007 allows the II-Group specimens to develop higher displacement ductility and deformability ratios than the control specimens. This demonstrates that the use of either SD685 or A1035 high-strength longitudinal reinforcement with reinforcing bar tensile strain of 0.007 at nominal flexural strength is capable of achieving comparable displace-

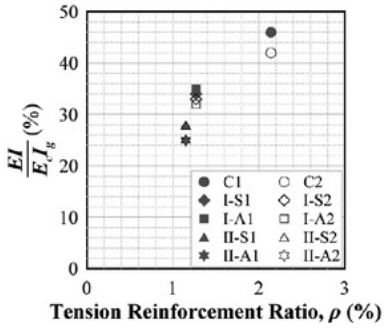

Fig. 7—Flexural rigidity ratio versus tension reinforcement ratio.

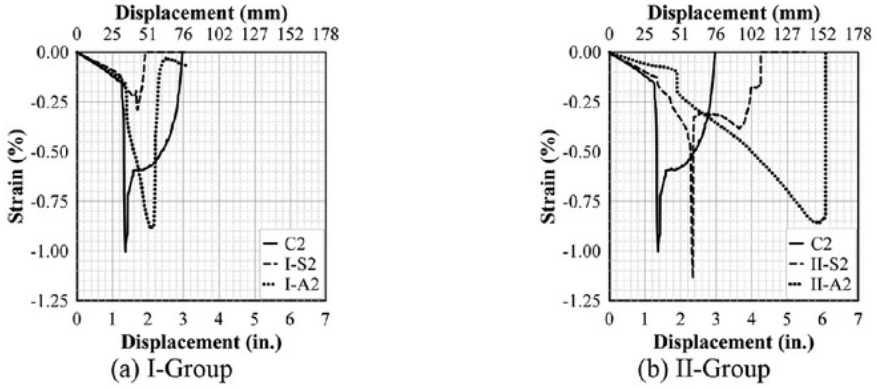

Fig. 8—Compression reinforcement strain gauge reading at LC4.

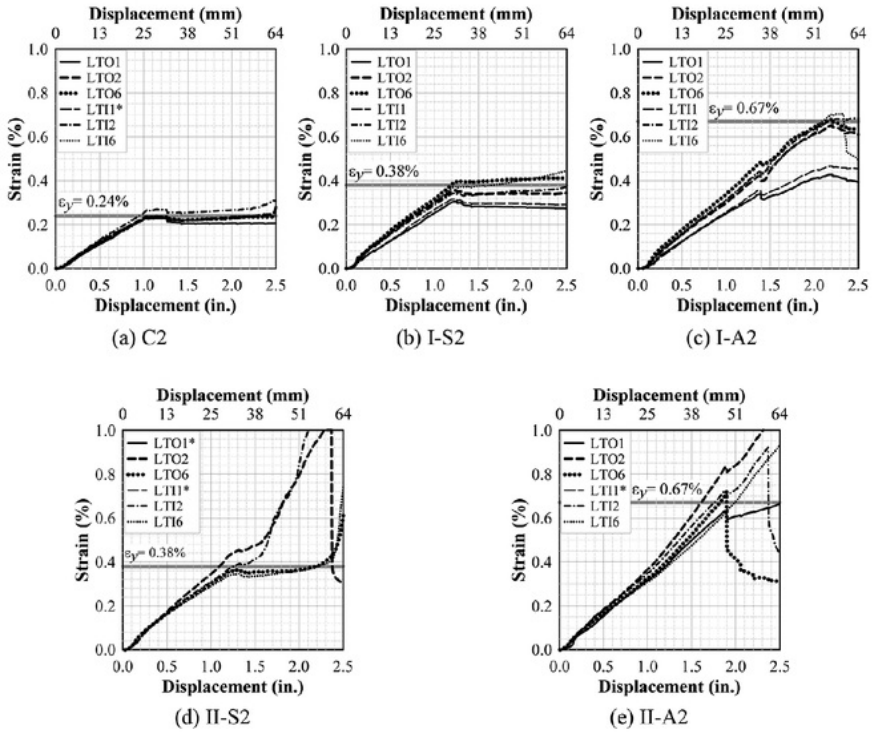

Fig. 9—Tension reinforcement strain gauge readings.

ment ductility and deformability ratios as the code-compliant control specimens using conventional Grade 60 longitudinal reinforcement with reinforcing bar tensile strain of 0.005 at nominal flexural strength. It should be reminded that reinforcing bar tensile strain at nominal flexural strength is estimated based on elastic-perfectly-plastic steel properties and is sensitive to the selected steel yield stress. Steel specified yield stress needs to be selected appropriately in the design phase to reflect the aforementioned findings. Comparing $\varepsilon_{t,b1}$ in Table 2 with $\varepsilon_{t,b2}$ in Table 5, it seems acceptable to assume steel specified yield stress of 100 ksi (690 MPa) for SD685 high-strength steel. However, for Grade 100 A1035 high-strength steel, test results suggest that specified steel specified yield stress of at least 120 ksi (830 MPa) may be conservative.

Stiffness

Specimens in the I-Group, designed to have equivalent flexural strengths as the control specimens, exhibit equivalent flexural rigidity ratio, EI/E_cI_g, of approximately 0.45, as shown in Table 5. The equivalent flexural rigidity ratios of II-Group specimens with larger cross sections are the lowest among the specimens. As depicted in Fig. 7, it is apparent that the equivalent flexural rigidity ratio is directly proportional to the tensile reinforcement ratio ρ.

Strain gauge readings

Representative compressive strain gauge readings at LC4 for Specimens C2, I-S2, I-A2, II-S2, and II-A2 are shown in Fig. 8. The commencement of cover concrete spalling is depicted by the first apparent kink of each curve. For all specimens except specimen pairs II-A1/A2, the sudden decrease of compressive strain after peak implies that buckling of compression reinforcement had occurred. It should be noted that strain gauge readings are sensitive to the crack locations, and the readings cannot be directly interpreted as the buckling strain for the corresponding longitudinal reinforcement. However, comparing the strain gauge readings in specimen pairs I-S1/S2 and I-A1/A2, it appears that A1035 steel buckles at a larger displacement demand than SD685 steel.

Most of the strain gauge readings on tension reinforcement exceed yield strain within the constant-moment region. Outside the constant-moment region, strain gauge readings on tension reinforcement with different stress-strain characteristics show different trends. A comparison of strain gauge readings outside the constant-moment region in the second specimen of each specimen pair is presented in Fig. 9. Broken strain gauge is indicated by an asterisk next to its label in the legend. As depicted in Fig. 9, readings of those strain gauges in the control specimens and specimen pair I-S1/S2 remain constant after spalling of cover concrete, which may indicate that the stress induced into the tension reinforcement is limited and the deformation is concentrated within the constant-moment region. The tensile stress is likely limited by the buckling of compression reinforcement, and the deformation increment within the constant-moment region may be attributed to the spread of plasticity as tension reinforcement goes through yield plateau at different locations. On the other hand, strain gauge readings on the A1035 tension reinforcement of specimen pair I-A1/A2 continue to increase until compression reinforcement buckles. For the

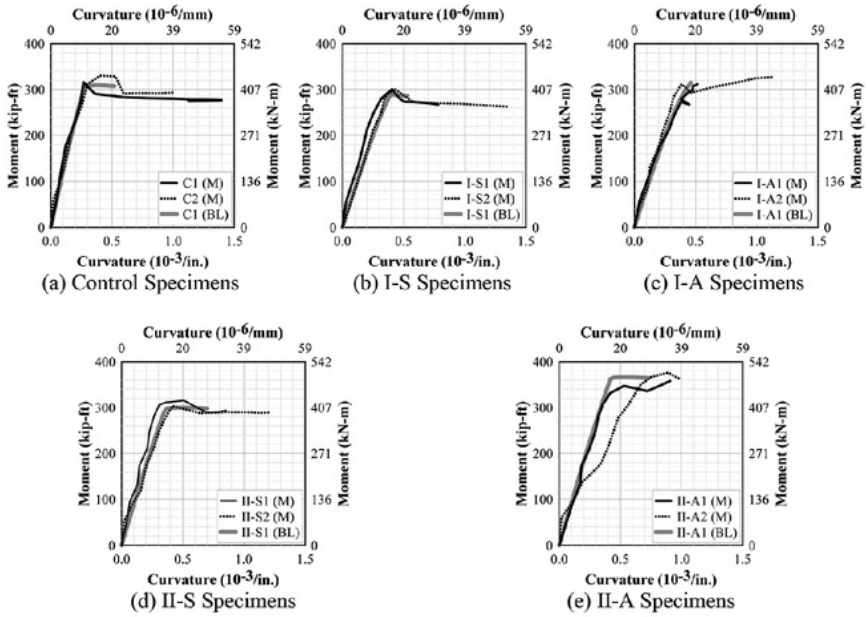

Fig. 10—Moment-curvature relationship comparison.

control and I-Group specimens, the farthest strain gauge that had recorded yield strain was located 4 in. (100 mm) outside the loading point. Strain gauge readings on the tension reinforcement of the II-Group specimens, as shown in Fig. 9, mostly exceed yield strain including the one located 14 in. (350 mm) outside the loading point.

Moment-curvature

The experimental moment-curvature response of each test specimen is presented in Fig. 10. The experimental curvature is estimated using optical markers within the constant-moment region—that is, grids B, C, and D, as shown in Fig. 3. All experimental moment-curvature curves are terminated at approximately 2.05 in. (52 mm) actuator displacement. Also shown in Fig. 10 are the theoretical moment-curvature response of the first specimens of each specimen pair. The theoretical curvature is constructed using tested material properties with concrete stress-strain relationship from Eq. (4) and elastic-perfectly-plastic steel properties. The theoretical curves are terminated at extreme concrete compressive strain of 0.003.

Analytical results indicate that experimental and theoretical moment-curvature relationships are in good agreement. This implies that the effective flexural stiffness may be satisfactorily estimated using moment-curvature analysis with elastic-perfectly-plastic properties for steels considered in this study. However, theoretical curvature at nominal flexural strength—that is, concrete compressive strain of 0.003—underestimates the ultimate curvature capacities for all specimens.

CONCLUSIONS

Test results from five pairs of RC beam specimens subjected to monotonically increasing gravity-type loading are reported. The main observations are summarized as follows:

1. Flexural strength of the I-Group specimens reinforced with either type of high-strength flexural reinforcement can be satisfactorily predicted using bilinear steel stress-strain relationships and equivalent concrete stress block per ACI 318-14, provided that steel yield stress is selected appropriately.

2. A maximum transverse reinforcement (Grade 60) spacing not exceeding $8d_b$ is suggested to restrain either SD685 or A1035 high-strength longitudinal reinforcement against premature buckling in flexural members primarily subjected to gravity-type loading, where d_b is the diameter of smallest compression reinforcement.

3. Control and I-Group specimens with similar reinforcing bar tensile strain at nominal flexural strength exhibited comparable ultimate displacement and failed in an identical failure mode.

4. If premature buckling of high-strength longitudinal reinforcement can be prevented, test results indicate that specimens using either SD685 or A1035 high-strength longitudinal reinforcement with reinforcing bar tensile strain of 0.007 at nominal flexural strength is capable of achieving comparable displacement ductility and deformability ratios as code-compliant control specimens using conventional Grade 60 longitudinal reinforcement with reinforcing bar tensile strain of 0.005 at nominal flexural strength.

5. Test results show that equivalent flexural rigidity ratio is proportional to the tension reinforcement ratio.

6. Analytical results indicate that the effective flexural stiffness may be satisfactorily estimated using moment-curvature analysis with elastic-perfectly-plastic properties for high-strength steels.

Readers should be reminded that findings of this study are based on limited test results and future studies are needed to verify the findings.

AUTHOR BIOS

ACI member **Marnie B. Giduquio** *is a PhD Student of civil and construction engineering at National Taiwan University of Science and Technology, Taipei, Taiwan. He received his BS in civil engineering from the University of San Carlos, Cebu City, Philippines, and his MS in civil and construction engineering from National Taiwan University of Science and Technology.*

ACI member **Min-Yuan Cheng** *is an Associate Professor of civil and construction engineering at National Taiwan University of Science and Technology. He is a member of ACI Subcommittee 318-J, Joints and Connections (Structural Concrete Building Code); and Joint ACI-ASCE Committee 352, Joints and Connections in Monolithic Concrete Structures.*

ACI member **Leonardus S. B. Wibowo** *is a PhD Student of civil and construction engineering at National Taiwan University of Science and Technology. He received his BS in civil engineering from Universitas Brawijaya, Malang, Indonesia, and his MS in civil engineering from Institut Teknologi Sepuluh Nopember, Surabaya, Indonesia.*

NOTATION

A_s	=	flexural reinforcement area
a	=	shear span, 63.0 in. (1600 mm)
d	=	specimen effective depth measured from extreme compression fiber to centroid of tension flexural reinforcement
d_b	=	diameter of minimum compression reinforcement
E_c	=	concrete modulus of elasticity, $57{,}000\sqrt{f_c'}$ (psi) ($4700\sqrt{f_c'}$ [MPa])
EI	=	specimen equivalent flexural rigidity
f_c	=	concrete compressive stress
f_c'	=	specified concrete compressive stress or cylinder average tested compressive stress
f_s	=	steel stress
f_{su}	=	steel coupon tensile stress corresponding to 10% drop from peak or at fracture
f_u	=	steel coupon peak tensile stress
f_y	=	specified yield stress or steel coupon tested yield stress
I_g	=	specimen gross moment of inertia
L	=	span length between simple supports, 157.0 in. (4000 mm)
M_B	=	tested flexural strength corresponding to Point B in Fig. 5
M_D	=	tested flexural strength corresponding to Point D in Fig. 5
$M_{n,a1}$	=	nominal flexural capacity using Eq. (1) to (4) with specified material properties
$M_{n,a2}$	=	nominal flexural capacity using elastic-perfectly-plastic steel response and equivalent concrete stress block with specified material properties
$M_{n,b2}$	=	nominal flexural capacity using elastic-perfectly-plastic steel response and equivalent concrete stress block with tested material properties
M_{peak}	=	specimen tested peak flexural strength—that is, either M_B or M_D
P_A to P_E	=	test loads corresponding to Points A to E of response curve in Fig. 5
P_y	=	idealized yield load
s	=	transverse reinforcement spacing, 5 in. (125 mm)
Δ_A to Δ_E	=	displacement at Points A to E of idealized load response, respectively
Δ_{Ser}	=	displacement under service load corresponding to $0.6M_{n,b2}$
Δ_y	=	idealized yield displacement
ε_c	=	concrete strain
ε_s	=	steel strain
ε_{sh}	=	steel coupon tensile strain at onset of strain hardening
ε_{su}	=	steel coupon strain corresponding to fracture stress f_{su}
$\varepsilon_{t,a1}$	=	outermost longitudinal steel tensile strain at nominal strength using Eq. (1) to (4) with specified material properties
$\varepsilon_{t,b1}$	=	outermost longitudinal steel tensile strain at nominal flexural strength using elastic-perfectly-plastic steel response and equivalent concrete stress block with specified material properties
$\varepsilon_{t,b2}$	=	outermost longitudinal steel tensile strain at nominal flexural strength using elastic-perfectly-plastic steel response and equivalent concrete stress block with tested material properties
ε_u	=	coupon steel strain corresponding to peak stress f_u
ε_y	=	steel coupon tensile yield strain
ρ	=	tension reinforcement ratio
ρ'	=	compression reinforcement ratio

REFERENCES

ACI Committee 318, 2014, "Building Code Requirements for Structural Concrete (ACI 318-14) and Commentary," American Concrete Institute, Farmington Hills, MI, 519 pp.

ACI Innovation Task Group 6, 2010, "Design Guide for the Use of ASTM A1035/A1035M Grade 100 (690) Steel Bars for Structural Concrete (ACI ITG-6R-10)," American Concrete Institute, Farmington Hills, MI, 2010, 90 pp.

Aoyama, H., 2001, "Design of Modern High-Rise Reinforced Concrete Structures," Series of Innovation in Structures and Construction, V. 3, Imperial College, London, UK, 442 pp.

ASTM A1035/A1035M-11, 2011, "Standard Specification for Deformed and Plain, Low-Carbon, Chromium, Steel Bars for Concrete Reinforcement," ASTM International, West Conshohocken, PA, 5 pp.

ASTM A370, 2012, "Standard Test Methods and Definitions for Mechanical Testing of Steel Products," ASTM International, West Conshohocken, PA, 48 pp.

ASTM A706/A706M, 2009, "Standard Specification for Low-Alloy Steel Deformed and Plain Bars for Concrete Reinforcement," ASTM International, West Conshohocken, PA, 6 pp.

Harries, K. A.; Shahrooz, B. M.; and Soltani, A., 2012, "Flexural Crack Widths in Concrete Girders with High-Strength Reinforcement," *Journal of Bridge Engineering*, ASCE, V. 17, No. 5, Sept.-Oct., pp. 804-812. doi: 10.1061/(ASCE)BE.1943-5592.0000306

Liel, A. B.; Haselton, C. B.; and Deierlein, G. G., 2011, "Seismic Collapse Safety of Reinforced Concrete Buildings. II: Comparative Assessment of Nonductile and Ductile Moment Frames," *Journal of Structural Engineering*, ASCE, V. 137, No. 4, Apr., pp. 492-502. doi: 10.1061/(ASCE)ST.1943-541X.0000275

Lin, C.-H., and Lee, F.-S., 2001, "Ductility of High-Performance Concrete Beams with High-Strength Lateral Reinforcement," *ACI Structural Journal*, V. 98, No. 4, July-Aug., pp. 600-608.

Mast, R. F.; Dawood, M.; Rizkalla, S. H.; and Zia, P., 2008, "Flexural Strength Design of Concrete Beams Reinforced with High Strength Steel Bars," *ACI Structural Journal*, V. 105, No. 5, Sept.-Oct., pp. 570-577.

Priestley, M. J. N.; Seible, F.; and Calvi, G. M., 1996, *Seismic Design and Retrofit of Bridges*, John Wiley & Sons, Inc., New York, 686 pp.

Rashid, M. A., and Mansur, M. A., 2005, "Reinforced High-Strength Concrete Beams in Flexure," *ACI Structural Journal*, V. 102, No. 3, May-June, pp. 462-471.

Shahrooz, B. M.; Miller, R. A.; Harries, K. A.; and Russell, H. G., 2011, "Design of Concrete Structures Using High-Strength Steel Reinforcement," *NCHRP Report 679*, Transportation Research Board, Washington DC, 72 pp.

Shahrooz, B. M.; Reis, J. M.; Wells, E. L.; Miller, R. A.; Harries, K. A.; and Russell, H. G., 2014, "Flexural Members with High-Strength Reinforcement: Behavior and Code Implications," *Journal of Bridge Engineering*, ASCE, V. 19, No. 5, May, 7 pp.

Sumpter, M. S.; Rizkalla, S. H.; and Zia, P., 2009, "Behavior of High-Performance Steel as Shear Reinforcement for Concrete Beams," *ACI Structural Journal*, ASCE, V. 106, No. 2, Mar.-Apr., pp. 171-177.

Wang, S.-C.; Lee, H.-J.; and Hwang, S.-J., 2009, "Mechanical Properties, Splice, and Anchorage of New High-Strength Reinforcing Bars," *Paper No. A-02*, TCI 2009 Concrete Technology Conference, 10 pp. (in Chinese).

2.HIGH-STRENGTH FLEXURAL REINFORCEMENT IN REINFORCED CONCRETE FLEXURAL MEMBERS UNDER MONOTONIC LOADING

ORIGINALITY REPORT

22%	18%	10%	11%
SIMILARITY INDEX	INTERNET SOURCES	PUBLICATIONS	STUDENT PAPERS

PRIMARY SOURCES

1	connection.ebscohost.com Internet Source	3%
2	kuscholarworks.ku.edu Internet Source	3%
3	Submitted to University of San Carlos Student Paper	2%
4	Submitted to University of Florida Student Paper	1%
5	dr.ntu.edu.sg Internet Source	1%
6	Submitted to University of Houston System Student Paper	1%
7	Min-Yuan Cheng, Rijalul Fikri, Cheng-Cheng Chen. "Experimental study of reinforced concrete and hybrid coupled shear wall systems", Engineering Structures, 2015 Publication	1%

8	www.dot.ca.gov Internet Source	1%
9	engineering.pitt.edu Internet Source	1%
10	repository.ntu.edu.sg Internet Source	1%
11	scholarbank.nus.edu.sg Internet Source	<1%
12	www.nehrp.gov Internet Source	<1%
13	www.engineering.pitt.edu Internet Source	<1%
14	repository.its.ac.id Internet Source	<1%
15	etds.lib.ncku.edu.tw Internet Source	<1%
16	"High Tech Concrete: Where Technology and Engineering Meet", Springer Nature, 2018 Publication	<1%
17	vdocuments.mx Internet Source	<1%
18	Seungwook Lim, Dan G. Zollinger. "Estimation of the Compressive Strength and Modulus of Elasticity of Cement-Treated Aggregate Base	<1%

Materials", Transportation Research Record: Journal of the Transportation Research Board, 2003
Publication

19	www.ce.ncsu.edu Internet Source	<1%
20	mmfx.com Internet Source	<1%
21	fedetd.mis.nsysu.edu.tw Internet Source	<1%
22	era.library.ualberta.ca Internet Source	<1%
23	cs.ru.nl Internet Source	<1%
24	www.pankowfoundation.org Internet Source	<1%
25	mitigation.eeri.org Internet Source	<1%
26	Galo Bowen, Paul Zheng, Cristopher D. Moen, Stephen R. Sharp. "Flexural Behavior at Service and Ultimate Limit State of One-Way Concrete Slabs Reinforced with Corrosion-Resistant Reinforcing Bars", Transportation Research Record: Journal of the Transportation Research Board, 2013 Publication	<1%

27	Maria S. Panfil. "Late Holocene stratigraphy of the Tetimpa archaeological sites, northeast flank of Popocatépetl volcano, central Mexico", Geological Society of America Bulletin, 02/1999 Publication	<1%
28	Bing Zhang. "The formation of the Hubble sequence of disc galaxies: the effects of early viscous evolution", Monthly Notices of the Royal Astronomical Society, 4/2000 Publication	<1%
29	www.nrmca.org Internet Source	<1%
30	Submitted to CSU, Fullerton Student Paper	<1%
31	www.ijaerd.co.in Internet Source	<1%
32	LeBorgne, M.R., and W.M. Ghannoum. "Calibrated analytical element for lateral-strength degradation of reinforced concrete columns", Engineering Structures, 2014. Publication	<1%
33	nardus.mpn.gov.rs Internet Source	<1%
34	C. C. Chen. "Formulas for Curvature Ductility Design of Doubly Reinforced Concrete Beams",	<1%

	Journal of Mechanics, 12/2004 Publication	
35	www.earthquakespectra.org Internet Source	<1%
36	www.civil.northwestern.edu Internet Source	<1%
37	"Titanium alloy bars for strengthening a reinforced concrete bridge", Sustainable Bridge Structures, 2015. Publication	<1%
38	digital.lib.washington.edu Internet Source	<1%
39	Manafpour, Ali Reza, and Parisa Kamrani Moghaddam. "Probabilistic Approach to Performance-Based Seismic Design of RC Frames", Vulnerability Uncertainty and Risk, 2014. Publication	<1%
40	s-space.snu.ac.kr Internet Source	<1%
41	www.jstage.jst.go.jp Internet Source	<1%
42	d-scholarship.pitt.edu Internet Source	<1%
43	www.mmfx.com	

Internet Source

<1%

---

44 repositories.lib.utexas.edu
Internet Source

<1%

---

45 S. J. Chen, K. C. Yang, K. M. Lin, C. D. Wang. "Seismic behavior of ductile rectangular composite bridge piers", Earthquake Engineering & Structural Dynamics, 2011
Publication

<1%

---

46 Moslehy, Yashar, Moheb Labib, and Ashraf Ayoub. "Evaluation of Softening-Coefficient in Reinforced Concrete Elements Retrofitted with FRP", Structures Congress 2010, 2010.
Publication

<1%

---

47 www.concrete.org
Internet Source

<1%

---

48 (Arsava, Tuğba and Baran, Eray). "Investigating Use Of Untensioned Prestressing Strands In Reinforced Concrete Flexural Members", Atılım Üniversitesi Açık Erişim Sistemi, 2011.
Publication

<1%

Exclude quotes	Off	Exclude matches	Off
Exclude bibliography	Off		

2.HIGH-STRENGTH FLEXURAL REINFORCEMENT IN REINFORCED CONCRETE FLEXURAL MEMBERS UNDER MONOTONIC LOADING

GRADEMARK REPORT

FINAL GRADE

/0

GENERAL COMMENTS

Instructor

PAGE 1

PAGE 2

PAGE 3

PAGE 4

PAGE 5

PAGE 6

PAGE 7

PAGE 8

PAGE 9

PAGE 10

PAGE 11